

Search for echoes on the edge of quantum black holes

Jahed Abedi^{1, 2, 3, 4, *}

¹Beijing Institute of Mathematical Sciences and Applications (BIMSA), Huairou District, Beijing 101408, P. R. China

²Department of Mathematics and Physics, University of Stavanger, NO-4036 Stavanger, Norway

³Albert-Einstein-Institut, Max-Planck-Institut für Gravitationsphysik, Callinstraße 38, 30167 Hannover, Germany

⁴Leibniz Universität Hannover, 30167 Hannover, Germany

I perform a template-based search for stimulated emission of Hawking radiation (or Boltzmann echoes) by combining the gravitational wave data from 47 binary black hole merger events observed by the LIGO-Virgo-KAGRA collaboration. With a Bayesian inference approach, I found no statistically significant evidence for this signal in either of the 3 Gravitational Wave Transient Catalogs GWTC-1, GWTC-2 and GWTC-3. While the data does not provide definitive evidence against the presence of Boltzmann echoes, the Bayesian evidence for most events falls within the range of 0.3–1.6, with the hypothesis of a common (non-vanishing) echo amplitude for all mergers being weakly disfavoured at 2:5 odds. The only exception is GW190521, the most massive and confidently detected event ever observed, which shows a positive evidence of 9.2 for stimulated Hawking radiation. The “look-elsewhere” effect for this outlier event is assessed by applying two distinct methods to add simulated signals in real data, before and after the event, giving false (true) positive detection probabilities for higher Bayes factors of $1.5^{+1.2}_{-0.9}\%$, $4.4^{+2.0}_{-2.0}\%$ ($35 \pm 7\%$, $35 \pm 15\%$). An optimal combination of posteriors yields an upper limit of $A < 0.4$ (at 90% confidence level) for a universal echo amplitude, whereas $A \sim 1$ was predicted in the canonical model. To ensure the robustness of the results, I have employed an additional method to combine the events hierarchically. This approach involves using a target gaussian distribution and extracting the parameters from multiple uncertain observations, which may be affected by selection biases.

I. INTRODUCTION

Post-merger gravitational wave (GW) echoes are our most direct observational windows into the quantum structure of black hole (BH) event horizons [1–3], while their non-existence would rule out different hypotheses about the nature of these enigmatic objects. The best view of these horizons can be achieved by combining a large number of binary black hole (BBH) merger events. As such, the GW data release for BBH mergers during the first, second and third observing run of LIGO/Virgo observatories [4–10] provides an unprecedented opportunity to test classical general relativity (GR), as well as its alternatives, in the strong gravity regime. One can assume GR as the base model and contrast it to GR+phenomenological echo waveforms to see which one fits the data better. Nonetheless, despite many attempts in searching for echoes [11–27] using different models, we still lack a waveform as physical/accurate as waveforms in GR. Additionally, there is no consensus on the optimal procedure to combine the events, for best sensitivity to fundamental physics. Although, the reported GW detections have so far been consistent with predictions of GR [8–10], the first search for echoes [11], motivated by a resolution to the BH quantum information paradox, was conducted for the first observing run of the Advanced LIGO detectors (O1), which then motivated further searches within different GW data analysis frameworks, and using more physical echo waveforms. Accordingly, several attempts with replication and extension were made with positive [11–15, 27], mixed [16–18],

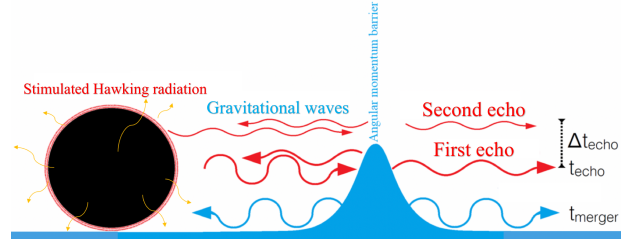


FIG. 1: Schematic diagram of GW echoes (stimulated Hawking radiation) from remnant of a BBH merger.

and negative [14, 19–22, 28, 29] results. These searches lead to tentative evidence and detection found with different groups [11–16, 18, 26, 27] at false alarm rates of 0.002% – 5% (but see [3, 16, 18, 30–33] for the ongoing discussion, comments, and rebuttals on statistical significance of these findings that motivate further investigations). So far, the searches for echoes have employed three strategies that can be classified into:

1. Waveform dependent [11, 14, 16, 17, 19, 21–23, 25, 26, 29].
2. Model-agnostic or coherent [12, 13, 15, 18, 24, 26–28].
3. Electromagnetic confirmation by Gill et al. [34].

For more details, discussions and review please see [3]. A confirmed detection of echoes would imply that the BH horizon is not totally absorbing. This would lead to post-merger repeating signals which are produced in the cavity that traps GWs between the classical angular momentum barrier and the near-horizon membrane/firewall

* jahed.abedi@bimsa.cn

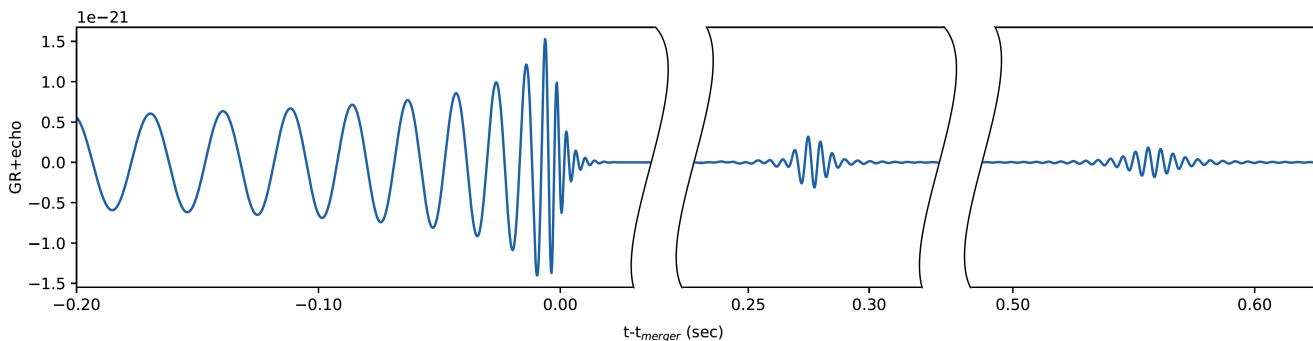


FIG. 2: Boltzmann GW echoes template for GW150914 like signal with amplitude $A = 1$.

[1, 2, 11, 26, 35]. However, firewalls are not a necessary condition to have observable echoes [36]. Stimulated emission of Hawking radiation, caused by the GWs that excite the quantum BH microstructure has a similar effect [26, 37–40]. As shown in Figs. 1 and 2, the trapped GWs slowly leak out, leading to repeating echoes within time intervals of:

$$\Delta t_{\text{echo}} \simeq \frac{4GM_{\text{BH}}}{c^3} \left(1 + \frac{1}{\sqrt{1-a^2}} \right) \times \ln \left(\frac{GM_{\text{BH}}}{c^2 \ell_{\text{QG}}} \right), \quad (1)$$

where M_{BH} and a are the mass and the dimensionless spin of the final BH remnant. Here, ℓ_{QG} is the characteristic physical length scale for quantum gravity effects where GWs are reflected near the (would-be) horizon. For $\ell_{\text{QG}} = \ell_{\text{Planck}}$, the reflection happens at a Planck distance from the horizon. More generally, for $\ell_{\text{QG}} = \ell_{\text{Planck}}/\Lambda$, deviations from GR happen sub-Planckian $\Lambda > 1$ or super-Planckian $\Lambda < 1$ scales. In this paper, we choose a conservative prior $-13 \leq \log_{10} \Lambda \leq 13$.

Here, in comparison to former attempts, I used a more physical waveform, based on stimulated Hawking radiation [37, 38] to test for the existence of echoes. Furthermore, I adopt the Bayesian methodology and p model, as in Abedi et al. [26].

In this approach, I set our model and search pipeline from a rather novel point of view to look for echoes combining 47 LVK BBH merger events, ensuring that these events meet the criterion, guaranteeing a false alarm rate $\text{FAR} < 10^{-3} \text{yr}^{-1}$. I perform the search for echoes on BBH signals using the GWTC-1 [4], GWTC-2 [5] and GWTC-3 [6]. This search includes almost the bulk of all the confident observations [4–6]. The missed events are either the marginal ones or needed a high computational cost (ones with very small mass). In this approach of combining events I assume echo model is the same for all the events. In particular, I assume all the events have same echo amplitude A . Although, this approach does not cover entire space of former searches, it makes a complementary search in overall.

One such proposal to search for quantum black holes in GW data is given by phenomenological Boltzmann echoes waveform [37, 38], where the general relativistic prediction for GW signal from BBH mergers $h_{\text{GR}}(\omega)$ in Fourier

space is modified to:

$$h_{\text{GR+echoes}}(A, \omega) = h_{\text{GR}}(\omega) \left[1 + Ae^{i\phi} \sum_{n=1}^{\infty} \mathcal{R}^n \right], \quad (2)$$

$$\mathcal{R} \equiv \exp \left[-\frac{\hbar|\omega - m\Omega_H|}{2kT_H} + i\omega\Delta t_{\text{echo}} \right], \quad (3)$$

where $Ae^{i\phi}$ quantifies their overall amplitude, while the modulus and phase of \mathcal{R} quantify their relative damping and temporal separation, respectively. Generally, we expect $0 \lesssim A \lesssim 2$ and $0 < \phi \leq 2\pi$ due to GR nonlinearities. Here T_H is Hawking temperature of the black hole. Furthermore, I set the horizon mode frequency $m \times \Omega_H$ to $m=2$ for quadrupolar gravitational radiation (with the assumption that the energy in BBH ringdown and echoes are dominated by this mode) as main frequency of search pipeline. In this search we only keep $n=2$ number of echoes. Note that the time window to look for echoes is dictated by the model in (3), where its dependence on Δt_{echo} and mass dependence is given by (1). In this equation the final mass of black hole M_{BH} is dictated by GR part of the event. The most physical and accurate term in this waveform is the Boltzmann factor \mathcal{R} which resembles the same factor in Hawking radiation process. This term is responsible to stimulated Hawking radiation making this process observable by gravitational wave detectors. Indeed, the remaining assumptions made in the construction of this phenomenological waveform are less accurate because achieving greater precision necessitates numerical relativity computations.

Although, there is no doubt that the $h_{\text{GR}}(\omega)$ (main event GR part) exists, we want to answer whether the echoes part exists. Existence of $h_{\text{GR}}(\omega)$ helps us to obtain physical prior for echo model i.e. improvements in priors for Δt_{echo} in (1) or Ω_H and T_H variables. Here, the Boltzmann factor $\exp[-\frac{\hbar|\omega - m\Omega_H|}{2kT_H}]$ originates from Hawking tunnelling rate to fuzzy states of quantum BH (please see Fig 2 for this waveform). Note that, repeating echoes time delay modifies this factor to $\exp[\frac{\omega - 2\Omega_H}{2T_H} + i\omega\Delta t_{\text{echo}}]$ [37, 38]. Here, I only keep first two echoes of the waveform in this search pipeline. Indeed, this waveform is not as perfect as GR waveform, while it helps us in future research and establishment of better waveforms.

Data presented in this paper and configuration files to replicate the results (including priors for GR parameters) available at [41].

Next section describes method and search pipeline and results. Section III provides an alternative approach to combine events hierarchically. Section IV, false/true positive estimations are provided for GW190521. Finally, I conclude with the search results and findings.

II. METHOD AND SEARCH PIPELINE AND RESULTS

I employed PyCBC inference [42] pipeline using a dynamic nested sampling algorithm, dynesty¹ [43]. It is based on sampling the likelihood function for a hypothesis that gives a measure of existence of a signal in the data. The likelihood function that requires a power spectral density (PSD) is supposed to be compatible with the natural assumption that the background is Gaussian. For further details and the definition of the likelihood function in PyCBC Inference, please refer to Section 2.2 of [42]. In order to combine the events, the amplitude A for all the 47 events (they are the events satisfy the criterion of a false alarm rate $\text{FAR} < 10^{-3}\text{yr}^{-1}$) is fixed to a universal value and the individual Bayes factors of events $B_{\text{Event}}(A)$ are combine as follows.

$$\text{Combined Bayes Factor} = B(A) = \prod_{i=\text{Events}} B_i(A), \quad (4)$$

where $B_i(A)$ is the Bayes factor of event i between the signal with echo hypothesis of amplitude A and noise. The combined Bayes factors is shown in Fig. 3.

I have used two/three detector networks H1-L1/H1-L1-V1 (Hanford, Livingston, Virgo) depending on the event and available data for this analyse [44]. While we know that LIGO/Virgo detectors are not stationary and/or Gaussian, as this was shown in [11] even for short range of data, we assume that the PSD around each event to be our safest choice. In order get a more accurate estimation of the likelihood, the PSDs of each event are obtained from data around each of the events which is $(-256, 256)$ second interval centered on merger. Note that there are some events that this range cannot be applicable due to each detector operation. So, in order to obtain the PSD around these events, this range is slightly adjusted. First I obtain the Bayes factor comparing the log likelihood to the log likelihood of the Gaussian noise. Then the combined Bayes factors of alternative models with different amplitude A are compared (here they are $h_{\text{GR}+\text{echoes}}(A, \omega)$ and $h_{\text{GR}+\text{echoes}}(A=0, \omega) = h_{\text{GR}}(\omega)$ in (2)). I used class of phenomenological IMR waveform family IMRPhenomPv2 [45, 46] which is freely available as part of LALSuite [47]. Although the main search in Abedi et al. [26] for GW190521 has been performed

with NRSur7dq4 waveform [48], in order to make identical search with other events in this paper I employed IMRPhenomPv2 for this event. The slight change in reported Bayes factor for this event in this paper is due to change in waveform. It is worth to mention that other waveforms/changes have shown consistent result for this event [26]. Note that the details on the results and smoke tests of the analysis for single event and its posterior for other parameters can be found in [26].

For each event I run for discrete set of amplitudes, where each run has different seed number. Since the Bayes factor estimation in PyCBC has error, it would be hard to read the result. Due to this error and in order to get smooth/stable result, for each amplitude A , the Bayes factor density $\bar{B}(A)$ which is the average of $B(A)$ within $(A - \Delta A/2, A + \Delta A/2)$ (see Fig. 3) evaluated. Although the lower ΔA gives a better resolution, it leads to more fluctuations and error. In order to improve the resolution one needs to increase the number of runs (increase the amplitude bins) as well, which leads to higher computational cost. So it requires a balance between computational cost and targeted resolution. In order to get a satisfying smoothness along with optimum computational cost $\Delta A = 0.2$ is chosen. In order to satisfy the approximation, three amplitude range is arranged. First range is near zero $A \sim 0$ which is the place of GR model for comparison. This range needs to have as high as possible runs to estimate the Bayes factor of GR accurately. I chose $A = (10^{-4}, 2 \times 10^{-4}, 3 \times 10^{-4}, 5 \times 10^{-4}, 10^{-3}, 2 \times 10^{-3}, 3 \times 10^{-3}, 5 \times 10^{-3})$ for amplitude bins to accomplish this task. Here the Bayes factor is re-normalized to $B(A \sim 0) = 1$. The second range is where the combined Bayes factor is $B(A) \geq 1$. This range is between $\sim (0, 0.5)$ with uniform intervals of $dA = 5 \times 10^{-3}$. In order to get satisfying result this range needs to have second priority in amplitude resolution. The last range where the Bayes factor drops significantly from 1 doesn't need to have high resolution as it already disfavoured by model when the events are combined. This range is between $(0.5, 2)$ with uniform intervals of $dA = 0.01$. However, for individual events one may need high resolution in all the amplitudes as well. I set 257 runs for each event and $47 \times 257 = 12079$ runs in total.

In order to obtain the overall Bayes factor of individual events and combined events we just do $\mathcal{B}_{\text{GR}}^{\text{GR}+\text{echo}} = \frac{1}{A_{\text{max}} - A_{\text{min}}} \int_{A_{\text{min}}}^{A_{\text{max}}} B(A) dA$ with $(A_{\text{min}}, A_{\text{max}}) = (0, 2)$. For combined events I got $\mathcal{B}_{\text{GR}}^{\text{GR}+\text{echo}} \simeq 0.4$. The result for individual events and their histogram are reported in Table I and Fig. 4 respectively.

It should be noted that the combined method presented here is insensitive to weak events. The insensitivity to weak events can be attributed to the nature of the amplitude A of the echo, which is relative to the main event signal amplitude. As events become weaker, the amplitude of the echo diminishes further into the noise. Consequently, the Bayes factor of an ideal weak event is $B(A)_{\text{zero amplitude event}} = 1$, making it without impact on (4). This implies that the hierarchy of events is already incorporated in this combined method.

¹ I used 25,000 live points in each run.

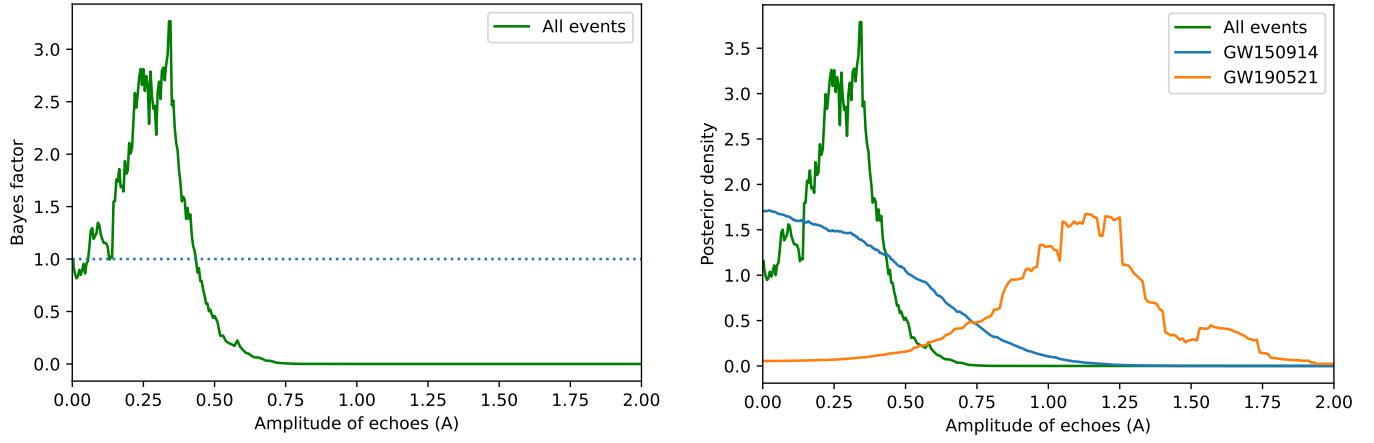


FIG. 3: (a): Combined Bayes factor density in terms of amplitude for 47 events. Combined events give an overall value of $\mathcal{B}_{\text{GR}}^{\text{GR+echo}} \simeq 0.4$ for Bayes factor. (b): Combined Bayes factor posterior density where the Bayes factor curves are normalized by $\int_{A_{\min}}^{A_{\max}} B(A)dA$. Here, in order to compare the individual events (GW150914 and GW190521) and combined events we plot the posterior density of the Bayes factors.

| | | | | | |
|-----------------|--|-----------------|--|-----------------|--|
| GWTC-1 | $\log_{10} \mathcal{B}_{\text{GR}}^{\text{GR+echo}}$ | GWTC-1 | $\log_{10} \mathcal{B}_{\text{GR}}^{\text{GR+echo}}$ | GWTC-1 | $\log_{10} \mathcal{B}_{\text{GR}}^{\text{GR+echo}}$ |
| GW150914 | -0.53 | GW170608 | 0.05 | GW170818 | -0.06 |
| GW151226 | -0.09 | GW170809 | 0.08 | GW170823 | -0.25 |
| GW170104 | 0.13 | GW170814 | -0.30 | | |
| GWTC-2 | $\log_{10} \mathcal{B}_{\text{GR}}^{\text{GR+echo}}$ | GWTC-2 | $\log_{10} \mathcal{B}_{\text{GR}}^{\text{GR+echo}}$ | GWTC-2 | $\log_{10} \mathcal{B}_{\text{GR}}^{\text{GR+echo}}$ |
| GW190408_181802 | -0.16 | GW190521 | 0.96 | GW190727_060333 | -0.30 |
| GW190412 | -0.09 | GW190521_074359 | -0.54 | GW190728_064510 | -0.01 |
| GW190421_213856 | 0.21 | GW190602_175927 | -0.22 | GW190814 | -0.42 |
| GW190503_185404 | -0.02 | GW190630_185205 | -0.17 | GW190828_063405 | 0.04 |
| GW190512_180714 | -0.06 | GW190706_222641 | -0.06 | GW190828_065509 | -0.14 |
| GW190513_205428 | -0.15 | GW190707_093326 | -0.02 | GW190910_112807 | -0.30 |
| GW190517_055101 | 0.07 | GW190708_232457 | -0.01 | GW190915_235702 | -0.09 |
| GW190519_153544 | -0.35 | GW190720_000836 | -0.07 | GW190924_021846 | 0.00 |
| GWTC-3 | $\log_{10} \mathcal{B}_{\text{GR}}^{\text{GR+echo}}$ | GWTC-3 | $\log_{10} \mathcal{B}_{\text{GR}}^{\text{GR+echo}}$ | GWTC-3 | $\log_{10} \mathcal{B}_{\text{GR}}^{\text{GR+echo}}$ |
| GW191109_010717 | -0.36 | GW191222_033537 | -0.32 | GW200219_094415 | -0.07 |
| GW191129_134029 | 0.01 | GW200112_155838 | -0.28 | GW200224_222234 | -0.34 |
| GW191204_171526 | 0.01 | GW200129_065458 | -0.43 | GW200225_060421 | -0.01 |
| GW191215_223052 | 0.2 | GW200202_154313 | 0.21 | GW200311_115853 | -0.37 |
| GW191216_213338 | 0.03 | GW200208_130117 | 0.08 | GW200316_215756 | -0.01 |

TABLE I: Results of Bayes factor for GW echoes in GWTC-1, GWTC-2, and GWTC-3 events. Positive value of the \log_{10} Bayes factor indicates a preference for the GR+echoes model over GR model, while the negative value suggests instead a preference for the GR model over the GR+echoes model. Here GW190521 shows loudest echo. Here based on [49] all the individual events appear as inconclusive to both GR or GR+echoes with GW190521 as exception! (see Fig. 4).

For further clarity, I summarize the data analysis steps as follows:

1. Perform the search for GR+echoes model (2) for discrete set of fixed amplitudes A within the prior range $0 \leq A \leq 2$. PyCBC software was utilized, as described in the first paragraph of this section.
2. Obtain the Bayes factors $B_i(A)$ of each run of event i and amplitude A for GR+echoes model.
3. For each event listed in Table I, calculate the Bayes factor by average integration over the amplitudes: $\mathcal{B}_{\text{GR}}^{\text{GR+echo}} = \frac{1}{A_{\max} - A_{\min}} \int_{A_{\min}}^{A_{\max}} B(A)dA$ with $(A_{\min}, A_{\max}) = (0, 2)$. The result is presented in Table I.
4. To obtain the combined Bayes factor, apply equation (4) using the Bayes factors obtained in step 2. The result is presented in Fig. 3.

The retrieved parameters and their associated er-

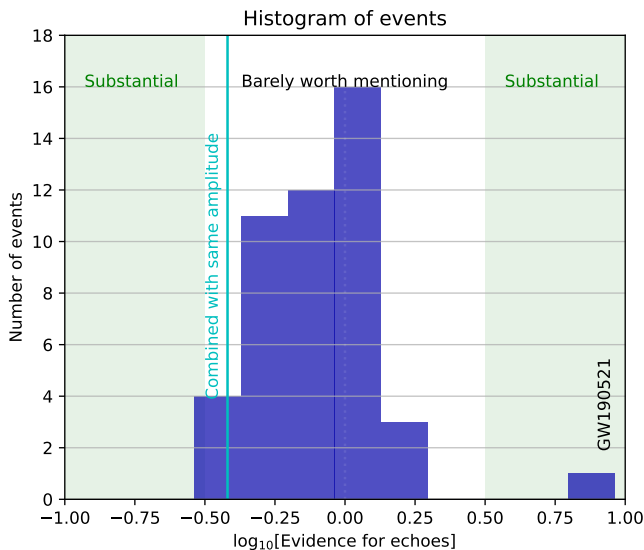


FIG. 4: Histogram of \log_{10} Bayes factors of 47 events in Table I. Vertical regions identify Jeffreys scale for interpretation of Bayes factor [49].

rors align well with the reported values for each event **GWOSC**.

Please note that as seen in (1) and (3) among the GR parameters directly impacting the redshifted final mass and final spin of the event (such as progenitor masses, redshift, and spin parameters) are the ones contributing most directly to the echo part of the waveform. On the other hand, parameters like inclination, right ascension, declination, polarization, and coalescence phase primarily assist in refining the error estimation of the aforementioned parameters, thus not directly impacting the echo part.

Let us compare the Bayes factors in Table I with the common events analyzed using p-value estimation by the LIGO-Virgo-KAGRA (LVK) Collaboration [25], as shown in Fig. 5. The plot in Fig. 5 also includes a degree 3 polynomial fit, suggesting a potential relationship between the LVK p-values and \log_{10} Bayes factors obtained from gravitational wave echo analysis. The scatter of points around the fit highlights residual variability, indicating that while a potential trend exists, other factors such as noise, the inherent complexity of gravitational wave signals, and differences in models and methods may influence the correlation.

III. COMBINATION OF BAYES FACTORS ASSUMING A TARGET DISTRIBUTION

This section, instead of using the hierarchical combination of Bayes factors as in the former approach, focuses on extracting distribution parameters from multiple uncertain observations that are subject to selection biases. To achieve this, I assume a target Gaussian distribution $\mathcal{P}(A, \bar{A}, \sigma) = e^{-(A-\bar{A})^2/2\sigma^2}/\sqrt{2\pi\sigma^2}$ with a mean of \bar{A} and

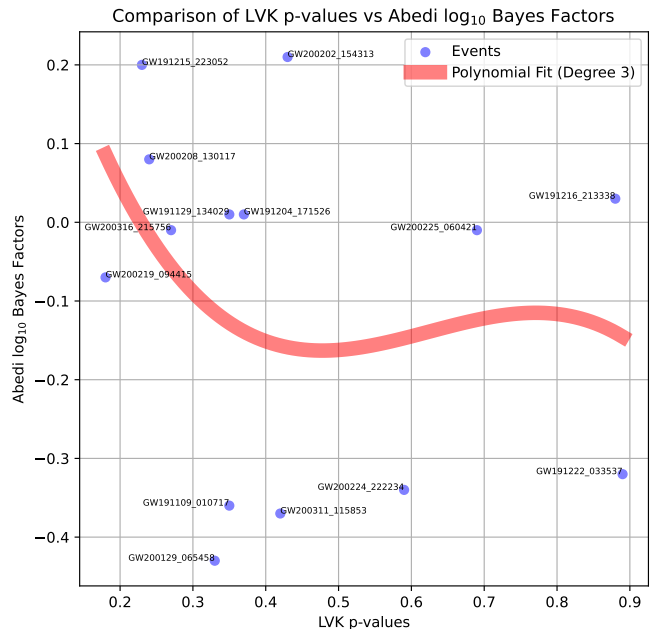


FIG. 5: Comparison of LVK p-values [25] and \log_{10} Bayes factors in Table I for common events, with a degree 3 polynomial fit illustrating their gradual relationship in gravitational wave echo analysis. The curved trend suggests a potential correlation, indicating that higher Bayes factors may correspond to lower p-values, despite differences in methods and models.

a standard deviation of σ for the measured parameter in this study. Then I combine them hierarchically [50, 51],

$$\mathcal{P}(\bar{A}, \sigma) = \int \prod_{i=\text{Events}} dA_i B_i(A_i) \bar{\mathcal{P}}(A_i, \bar{A}, \sigma) \quad (5)$$

Here, $\mathcal{P}(\bar{A}, \sigma)$ gives a posterior function for hierarchical combination of events for parameters \bar{A} and σ . With the above choice of likelihood and $\sigma \rightarrow 0$, our hierarchical approach reduces to the combined Bayes factor method described in (4) for combining events. This can be seen in Fig. 6, as we approach $\sigma \rightarrow 0$ limit, it tends to Fig. 3 for all events. Fig. 6 presents the extracted parameters \bar{A} and σ obtained from this analysis. In this plot the lower value of 0.05 for σ is implemented to avoid errors caused by the Bayes factor. As it can be seen in this plot, peak of \bar{A} is consistent with Fig. 3 while σ peaks near zero. This shows that there is no spread between events.

IV. FALSE POSITIVE AND TRUE POSITIVE ESTIMATION FOR GW190521

In this section, false/true positive probabilities for GW190521 are calculated. As Table I confirms evidence in favour of echoes for this event, this section provides supplementary validation for the obtained results.

To ensure a robust outcome, I utilized two distinct approaches to obtain false and true positives. In the following subsections both of the methods are explained.

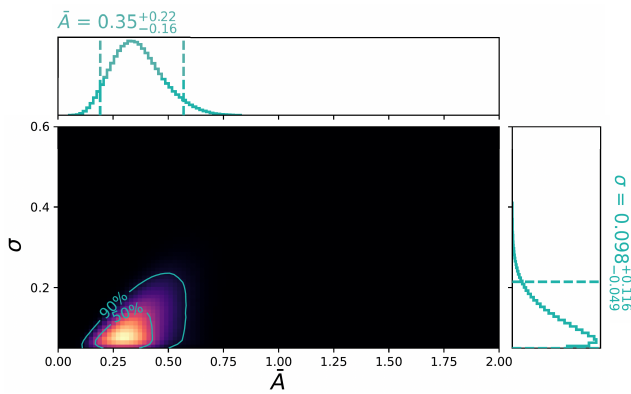


FIG. 6: Posterior for extracted parameters \bar{A} and σ from target distribution $\bar{\mathcal{P}}(\bar{A}, \bar{\sigma})$ for 47 events conducted in this paper.

A. Using samples from GR posterior

This is the same analysis performed in [26]. In this section we perform the analysis using NRSur7dq4 waveform [48]. Thus, for consistency the Bayes factors of injections are compared to the one obtained with this waveform. Even though this section focuses on the outcome of the single event GW190521, it satisfies the validation test for ensuring the proper functioning of the method and model. Since in this section we don't need to combine events and making a grid for amplitude A as the former section, I made it as free parameter inside its prior range of the model $0 \leq A \leq 2$. In order to evaluate the true positive we have to inject GR models containing echoes. The GR only model for injections are drawn from random samples given by GR posterior, which is obtained from 10 different seed runs. Note that in the GR run, due to the marginalization over the coalescence phase of the binary, this particular parameter was not included in the corresponding posterior sample. As a result, the random samples consist of 14 parameters, and the coalescence phase was estimated additionally using waveform fitting to the data. Once the GR part is selected out of random samples of its posterior, the echo part is added. The echo part is within a random selection from uniform priors of $-13 \leq \log_{10} \Lambda \leq 13$, $0 \leq A \leq 2$, and $0 \leq \phi \leq 2\pi$ which is given in first section. In order to evaluate the background and minimize non-Gaussian and/or non-stationary effects the data around the event is being used. Therefore, they are injected at random offset times of $\pm[5, 32]$ sec compared to GW190521 merger time. The gap ± 5 sec around GW190521 is due to preventing any contamination of data. In order to compare the foreground (true positive) to the background (false positive), I also injected a sample with zero echo amplitude for any corresponding GR+echo injection at the same offset time. In the next step run the same script job for injections with GR+echo and GR waveform. The number of injections performed for zero amplitude echoes (GR waveforms) is 343, while this number is 110 for non-zero amplitude echoes (GR+echo waveform). Fig.

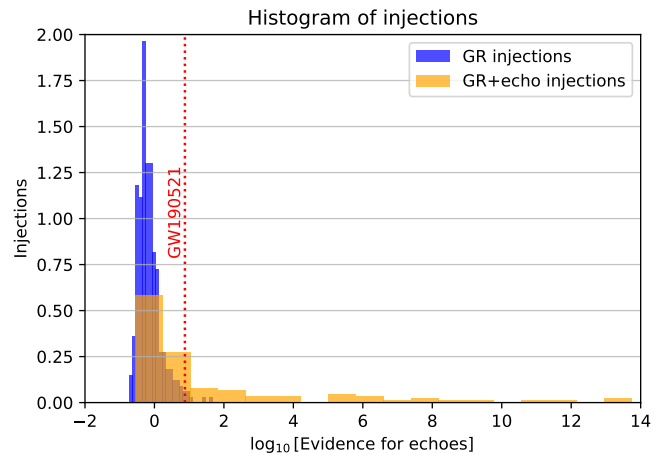


FIG. 7: Histograms to quantify false positive (GR injections) and true positive (GR+echo injections). Comparing to the GW190521 echo, we obtain their values as $1.46^{+1.17}_{-0.875}\%$, and $34.5 \pm 7.3\%$ respectively.

7 is the results of this analysis in a histogram plot. We find injection Bayes factor for GR+echo with $34.5 \pm 7.3\%$ and GR with $1.46^{+1.17}_{-0.88}\%$ being larger than $\mathcal{B} = 7.5$ the echo Bayes factor for GW190521 with NRSur7dq4 waveform [26]. Then the empirical likelihood ratio = $24.3^{+42.7}_{-11.8}$ which is the ratio of the foreground probability to the background probability is obtained. Please note that the errors associated with these estimates, as well as those in the subsequent subsection, are calculated using Bootstrapping.

B. Using GW190521 signal

In this part, we employ an alternative approach to generate foregrounds and backgrounds for injections, eliminating the need for a waveform model for the GR part to generate these injections. Specifically, we extract the data strain associated with the GW190521 main event signal and add it with or without echoes into various sections of the data surrounding the event. By employing this approach, we aim to preserve the impact of the “main” GW190521 signal on the Bayes factor, focusing solely on injecting the echo part into nearby data, with or without echoes.

In this approach, a Gaussian window function is utilized to extract the main event signal

$$\exp\left(-\frac{(t - t_{\text{merger}})^2}{\sigma^2}\right) \times \begin{pmatrix} \text{Hanford data} \\ \text{Livingston data} \\ \text{Virgo data} \end{pmatrix} \quad (6)$$

where $t_{\text{merger}} = 1242442967.4$ sec (GPS time). The parameter σ should be taken in such that covers the main event signal and doesn't leak to ~ 1 sec echo range. Thus $\sigma = 0.5$ sec is chosen. Then instead of GR part in former section we replace it with this extracted signal.

After preparing the injections, we follow the same procedure as described earlier, running the script for

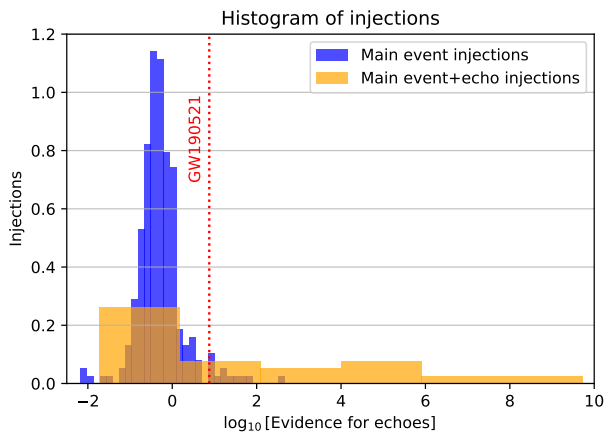


FIG. 8: Histograms to quantify false positive (main event injections) and true positive (main event+echo injections). Comparing to the GW190521 echo, we obtain their values as $4.4_{-2.0}^{+2.0}\%$, and $35 \pm 15\%$ respectively.

injections using both the GR+echo and GR waveforms. A total of 250 injections are performed for zero-amplitude echoes (main event injections), while 20 injections are conducted for non-zero amplitude echoes (main event+echo injections). The results of this analysis are presented in Fig. 8 as a histogram plot. We observe that the injection Bayes factor for the main event+echo injections and for main event injections being larger than $\mathcal{B} = 7.5$ (echo Bayes factor for GW190521 with the NR-Sur7dq4 waveform [26]) is $35 \pm 15\%$, and $4.4_{-2.0}^{+2.0}\%$ respectively. Subsequently, we calculate the empirical likelihood ratio as $7.8_{-4.0}^{+7.8}$, representing the ratio of foreground probability to background probability.

It is important to note that here we observe a false-positive rate three times higher than that in the previous subsection. This higher rate could be due to the windowing of the main event signal, which includes unavoidable additional noise around the main event in this approach. In other words, it introduces additional noise into the analysis.

V. CONCLUSION AND DISCUSSIONS

I presented the outcome which gives measure of possibility for preference of $h_{\text{GR}+\text{echoes}}$ over h_{GR} based on Bayes factors comparison of these two models. The 47 analysed events in Table I and Fig. 4 for individual events show inconclusive result in preference for GR or GR+echo, although with slight preference for GR but not by much. The main scope and result of the paper is combination of echoes for large number of events. We see that the combined Bayes factor which is $\mathcal{B}_{\text{GR}}^{\text{GR}+\text{echo}} \simeq 0.4$ is still inconclusive about GR+echo and GR. It is realised that this combining method gives four order of magnitude higher Bayes factor compared to when we simply combine the individual events Bayes factor via

multiplication $\prod_{i=\text{Events}} \mathcal{B}_i^{\text{GR}+\text{echo}} = 3 \times 10^{-5}$. In another words the fact that the combined Bayes factor for preference to GR has dropped from $\sim 3.3 \times 10^4$ to ~ 2.5 indicates that there are still much to do in method improvement. Additionally, the large number of events and computational costs is a guarantee against Bayes factor hack making the result robust.

The only event that has shown evidence for preference of GR+echo model is GW190521 with $\mathcal{B}_{\text{GR}}^{\text{GR}+\text{echo}} = 9.2$ (see Fig. 4). This is the most massive and confidently detected BBH merger event observed to date [5]. The remarkably loud ringdown of this event warrants special attention, making it a prime candidate for investigating gravitational wave echoes. After conducting a thorough analysis of this outlier event using two distinct methods, I found false detection probabilities of $1.46_{-0.88}^{+1.17}\%$ and $4.4_{-2.0}^{+2.0}\%$. The ratio of foreground probability to background in each case yielded an empirical likelihood ratio of $24.3_{-11.8}^{+2.7}$ and $7.8_{-4.0}^{+7.8}$. I refer the detailed interpretation and investigation about this event to Abedi et al. [26].

Presuming a simple speculation that we can compare all the events as same (echo model remain same for all the 47 events and their echo amplitudes compare to main event amplitude doesn't change by much despite the change in initial condition of the progenitor BBH mergers) and all the 47 BBH events should show evidence for echo signals in this model and the space of parameters considered in this search, I found an upper bound amplitude $A < 0.4$ (at 90% confidence level) for echoes. I remind the reader that bounds from our search only relate to the family of echo waveforms considered here.

Additionally, I employed an additional method to combine the events, wherein the parameters are extracted from multiple uncertain observations affected by selection biases. In this approach, a target distribution of Gaussian with mean \bar{A} and standard deviation σ for the search parameter A is assumed. Then I combine them hierarchically as shown in (5). Although the extracted parameter \bar{A} and its error, as depicted in Fig. 6, is consistent with the peak observed for echo amplitude in Fig. 3, the extracted parameter σ shows that there is no significant spread between events.

It is worth to note that I didn't see any evidence for echoes in O1 in contrast to [11, 16, 17], possibly because the model I used here is different and has much suppressed amplitudes in contrast to ADA model in [11].

It is crucial to underscore that, considering the present sensitivity levels of gravitational wave detectors [52, 53], there's no concrete evidence of stimulated Hawking radiation from black hole mergers or Boltzmann echoes at $\geq 5\sigma$. Taking a cautious approach, this analysis stands as the most stringent constraint on the amplitude of this signal to date.

In order to do a better search for quieter echoes, we might need to have a more physical echo waveforms. In another words, concrete models from alternatives to GR are needed to use in PyCBC pipeline. Without better

models, we might wait for O4. Observations will improve in number. LISA, Einstein Telescope, and Cosmic Explorer will make a big breakthrough in sensitivity in search for alternatives to GR.

ACKNOWLEDGMENTS

I would like to thank Niayesh Afshordi and Alex B. Nielsen for helpful comments and discussions. I also thank Conner Dailey for suggestion about Fig. 2. I thank the Max Planck Gesellschaft and the Atlas cluster computing team at AEI Hannover for support and compu-

tational help. I was supported by ROMFORSK grant Project. No. 302640. This research has made use of data, software and/or web tools obtained from the Gravitational Wave Open Science Center (<https://www.gwopenscience.org>), a service of LIGO Laboratory, the LIGO Scientific Collaboration and the Virgo Collaboration. LIGO is funded by the U.S. National Science Foundation. Virgo is funded by the French Centre National de Recherche Scientifique (CNRS), the Italian Istituto Nazionale della Fisica Nucleare (INFN) and the Dutch Nikhef, with contributions by Polish and Hungarian institutes.

-
- [1] V. Cardoso, E. Franzin, and P. Pani, *Phys. Rev. Lett.* **116**, 171101 (2016), [Erratum: *Phys. Rev. Lett.* 117, no.8, 089902 (2016)], [arXiv:1602.07309 \[gr-qc\]](https://arxiv.org/abs/1602.07309).
- [2] V. Cardoso, S. Hopper, C. F. B. Macedo, C. Palenzuela, and P. Pani, *Phys. Rev.* **D94**, 084031 (2016), [arXiv:1608.08637 \[gr-qc\]](https://arxiv.org/abs/1608.08637).
- [3] J. Abedi, N. Afshordi, N. Oshita, and Q. Wang, *Universe* **6**, 43 (2020), [arXiv:2001.09553 \[gr-qc\]](https://arxiv.org/abs/2001.09553).
- [4] B. Abbott et al. (LIGO Scientific, Virgo), *Phys. Rev. X* **9**, 031040 (2019), [arXiv:1811.12907 \[astro-ph.HE\]](https://arxiv.org/abs/1811.12907).
- [5] R. Abbott et al. (LIGO Scientific, Virgo), *Phys. Rev. X* **11**, 021053 (2021), [arXiv:2010.14527 \[gr-qc\]](https://arxiv.org/abs/2010.14527).
- [6] R. Abbott et al. (LIGO Scientific, VIRGO, KAGRA), (2021), [arXiv:2111.03606 \[gr-qc\]](https://arxiv.org/abs/2111.03606).
- [7] B. P. Abbott et al. (Virgo, LIGO Scientific), *Phys. Rev. Lett.* **116**, 061102 (2016), [arXiv:1602.03837 \[gr-qc\]](https://arxiv.org/abs/1602.03837).
- [8] B. P. Abbott et al. (Virgo, LIGO Scientific), *Phys. Rev. Lett.* **116**, 221101 (2016), [arXiv:1602.03841 \[gr-qc\]](https://arxiv.org/abs/1602.03841).
- [9] B. P. Abbott et al. (LIGO Scientific, VIRGO), *Phys. Rev. Lett.* **118**, 221101 (2017), [Erratum: *Phys. Rev. Lett.* 121, no.12, 129901 (2018)], [arXiv:1706.01812 \[gr-qc\]](https://arxiv.org/abs/1706.01812).
- [10] B. P. Abbott et al. (LIGO Scientific, Virgo), *Phys. Rev. Lett.* **123**, 011102 (2019), [arXiv:1811.00364 \[gr-qc\]](https://arxiv.org/abs/1811.00364).
- [11] J. Abedi, H. Dykaar, and N. Afshordi, *Phys. Rev.* **D96**, 082004 (2017), [arXiv:1612.00266 \[gr-qc\]](https://arxiv.org/abs/1612.00266).
- [12] R. S. Conklin, B. Holdom, and J. Ren, *Phys. Rev.* **D98**, 044021 (2018), [arXiv:1712.06517 \[gr-qc\]](https://arxiv.org/abs/1712.06517).
- [13] J. Abedi and N. Afshordi, *JCAP* **1911**, 010 (2019), [arXiv:1803.10454 \[gr-qc\]](https://arxiv.org/abs/1803.10454).
- [14] N. Uchikata, H. Nakano, T. Narikawa, N. Sago, H. Tagoshi, and T. Tanaka, *Phys. Rev.* **D100**, 062006 (2019), [arXiv:1906.00838 \[gr-qc\]](https://arxiv.org/abs/1906.00838).
- [15] B. Holdom, *Phys. Rev. D* **101**, 064063 (2020), [arXiv:1909.11801 \[gr-qc\]](https://arxiv.org/abs/1909.11801).
- [16] J. Westerweck, A. Nielsen, O. Fischer-Birnholtz, M. Cabero, C. Capano, T. Dent, B. Krishnan, G. Meadors, and A. H. Nitz, *Phys. Rev.* **D97**, 124037 (2018), [arXiv:1712.09966 \[gr-qc\]](https://arxiv.org/abs/1712.09966).
- [17] A. B. Nielsen, C. D. Capano, O. Birnholtz, and J. Westerweck, *Phys. Rev.* **D99**, 104012 (2019), [arXiv:1811.04904 \[gr-qc\]](https://arxiv.org/abs/1811.04904).
- [18] F. Salemi, E. Milotti, G. A. Prodi, G. Vedovato, C. Lazzaro, S. Tiwari, S. Vinciguerra, M. Drago, and S. Klimentenko, *Phys. Rev.* **D100**, 042003 (2019), [arXiv:1905.09260 \[gr-qc\]](https://arxiv.org/abs/1905.09260).
- [19] R. K. L. Lo, T. G. F. Li, and A. J. Weinstein, *Phys. Rev.* **D99**, 084052 (2019), [arXiv:1811.07431 \[gr-qc\]](https://arxiv.org/abs/1811.07431).
- [20] K. W. Tsang, A. Ghosh, A. Samajdar, K. Chatziioannou, S. Mastrogiovanni, M. Agathos, and C. Van Den Broeck, (2019), [arXiv:1906.11168 \[gr-qc\]](https://arxiv.org/abs/1906.11168).
- [21] R. Abbott et al. (LIGO Scientific, Virgo), (2020), [arXiv:2010.14529 \[gr-qc\]](https://arxiv.org/abs/2010.14529).
- [22] Y.-T. Wang and Y.-S. Piao, (2020), [arXiv:2010.07663 \[gr-qc\]](https://arxiv.org/abs/2010.07663).
- [23] J. Westerweck, Y. Sherf, C. D. Capano, and R. Brustein, (2021), [arXiv:2108.08823 \[gr-qc\]](https://arxiv.org/abs/2108.08823).
- [24] J. Ren and D. Wu, *Phys. Rev. D* **104**, 124023 (2021), [arXiv:2108.01820 \[gr-qc\]](https://arxiv.org/abs/2108.01820).
- [25] R. Abbott et al. (LIGO Scientific, VIRGO, KAGRA), (2021), [arXiv:2112.06861 \[gr-qc\]](https://arxiv.org/abs/2112.06861).
- [26] J. Abedi, L. F. L. Micchi, and N. Afshordi, (2021), [arXiv:2201.00047 \[gr-qc\]](https://arxiv.org/abs/2201.00047).
- [27] R. S. Conklin and N. Afshordi, (2021), [arXiv:2201.00027 \[gr-qc\]](https://arxiv.org/abs/2201.00027).
- [28] A. Miani, C. Lazzaro, G. A. Prodi, S. Tiwari, M. Drago, E. Milotti, and G. Vedovato, *Phys. Rev. D* **108**, 064018 (2023), [arXiv:2302.12158 \[gr-qc\]](https://arxiv.org/abs/2302.12158).
- [29] N. Uchikata, T. Narikawa, H. Nakano, N. Sago, H. Tagoshi, and T. Tanaka, *Phys. Rev. D* **108**, 104040 (2023), [arXiv:2309.01894 \[gr-qc\]](https://arxiv.org/abs/2309.01894).
- [30] G. Ashton, O. Birnholtz, M. Cabero, C. Capano, T. Dent, B. Krishnan, G. D. Meadors, A. B. Nielsen, A. Nitz, and J. Westerweck, (2016), [arXiv:1612.05625 \[gr-qc\]](https://arxiv.org/abs/1612.05625).
- [31] J. Abedi, H. Dykaar, and N. Afshordi, (2017), [arXiv:1701.03485 \[gr-qc\]](https://arxiv.org/abs/1701.03485).
- [32] J. Abedi, H. Dykaar, and N. Afshordi, (2018), [arXiv:1803.08565 \[gr-qc\]](https://arxiv.org/abs/1803.08565).
- [33] J. Abedi and N. Afshordi, (2020), [arXiv:2001.00821 \[gr-qc\]](https://arxiv.org/abs/2001.00821).
- [34] R. Gill, A. Nathanail, and L. Rezzolla, *Astrophys. J.* **876**, 139 (2019), [arXiv:1901.04138 \[astro-ph.HE\]](https://arxiv.org/abs/1901.04138).
- [35] Q. Wang and N. Afshordi, *Phys. Rev.* **D97**, 124044 (2018), [arXiv:1803.02845 \[gr-qc\]](https://arxiv.org/abs/1803.02845).
- [36] J. Abedi, (2022), [arXiv:2209.07363 \[hep-th\]](https://arxiv.org/abs/2209.07363).
- [37] N. Oshita, Q. Wang, and N. Afshordi, *JCAP* **04**, 016 (2020), [arXiv:1905.00464 \[hep-th\]](https://arxiv.org/abs/1905.00464).
- [38] Q. Wang, N. Oshita, and N. Afshordi, (2019), [arXiv:1905.00446 \[gr-qc\]](https://arxiv.org/abs/1905.00446).
- [39] S. Xin, B. Chen, R. K. L. Lo, L. Sun, W.-B. Han, X. Zhong, M. Srivastava, S. Ma, Q. Wang, and Y. Chen, *Phys. Rev. D* **104**, 104005 (2021), [arXiv:2105.12313 \[gr-qc\]](https://arxiv.org/abs/2105.12313).

- [40] M. Srivastava and Y. Chen, *Phys. Rev. D* **104**, 104006 (2021), arXiv:2108.01329 [gr-qc].
- [41] “Data and codes for arXiv:2301.00025,” <https://github.com/jahedabedi/Search-for-echoes-on-the-edge-of-quantum-black-holes>
- [42] C. M. Biwer, C. D. Capano, S. De, M. Cabero, D. A. Brown, A. H. Nitz, and V. Raymond, *Publ. Astron. Soc. Pac.* **131**, 024503 (2019), arXiv:1807.10312 [astro-ph.IM].
- [43] J. S. Speagle, *Monthly Notices of the Royal Astronomical Society* **493**, 3132–3158 (2020).
- [44] “The gravitational-wave transient catalog (gwtc),” <https://gwosc.org/eventapi/html/GWTC/>.
- [45] S. Khan, S. Husa, M. Hannam, F. Ohme, M. Pürrer, X. Jiménez Forteza, and A. Bohé, *Phys. Rev. D* **93**, 044007 (2016), arXiv:1508.07253 [gr-qc].
- [46] M. Hannam, P. Schmidt, A. Bohé, L. Haegel, S. Husa, F. Ohme, G. Pratten, and M. Pürrer, *Phys. Rev. Lett.* **113**, 151101 (2014), arXiv:1308.3271 [gr-qc].
- [47] “Ligo scientific collaboration (2018), ligo algorithm library,” <https://git.ligo.org/lscsoft/lalsuite>.
- [48] V. Varma, S. E. Field, M. A. Scheel, J. Blackman, D. Gerosa, L. C. Stein, L. E. Kidder, and H. P. Pfeiffer, *Phys. Rev. Research* **1**, 033015 (2019).
- [49] R. E. Kass and A. E. Raftery, *Journal of the American Statistical Association* **90**, 773 (1995).
- [50] M. Isi, K. Chatziioannou, and W. M. Farr, *Phys. Rev. Lett.* **123**, 121101 (2019), arXiv:1904.08011 [gr-qc].
- [51] I. Mandel, W. M. Farr, and J. R. Gair, *Mon. Not. Roy. Astron. Soc.* **486**, 1086 (2019), arXiv:1809.02063 [physics.data-an].
- [52] L. F. Longo Micchi, N. Afshordi, and C. Chirenti, *Phys. Rev. D* **103**, 044028 (2021), arXiv:2010.14578 [gr-qc].
- [53] S. Ma, Q. Wang, N. Deppe, F. Hébert, L. E. Kidder, J. Moxon, W. Throwe, N. L. Vu, M. A. Scheel, and Y. Chen, *Phys. Rev. D* **105**, 104007 (2022), arXiv:2203.03174 [gr-qc].